IEEE Access
Multidisciplinary | Rapid Review | Open Access Journal

SPECIAL SECTION ON ADVANCED OPTICAL IMAGING FOR EXTREME ENVIRONMENTS

Received September 9, 2019, accepted September 27, 2019, date of publication November 1, 2019,
date of current version November 13, 2019.

Digital Object Identifier 10.1109/ACCESS.2019.2950896

Active Mode Single Pixel Imaging in the Highly Turbid Water Environment Using Compressive Sensing

QI CHEN[1,2], SANDEEP KUMAR CHAMOLI[2,3], PENG YIN[1,2], XIN WANG[2], AND XIPING XU[1]

[1]College of Optoelectronic Engineering, Changchun University of Science and Technology, Changchun 130022, China
[2]School of Engineering, Monash University Malaysia, Bandar Sunway 47500, Malaysia
[3]The Guo China-US Photonics Laboratory, State Key Laboratory of Applied Optics, Changchun Institute of Optics, Fine Mechanics and Physics, Chinese Academy of Sciences, Changchun 130033, China

Corresponding author: Xiping Xu (1772318932@qq.com)

This work was supported in part by the National Natural Science Foundation of China under Grant 61803045 and Grant 61605016, in part by the Ministry of Higher Education, Malaysia, under Grant FRGS/1/2016/STG02/ MUSM/02/1, and in part by the Science and Technology Development Plan of Jilin Province of China under Grant 20160520175JH.

ABSTRACT Underwater imaging has always been a challenge due to limitations imposed by scattering and absorption nature of the underwater environment. The light would be highly degraded after reflection and propagation in the water medium. Being an advanced imaging technique, Single-pixel Imaging (SPI) is applicable to acquire object spatial information in low light, severe backscattering, and high absorption conditions. Combination of Compressive Sensing (CS) and SPI can overcome the limitation of SPI algorithms such as long data-acquisition time, low reconstruction efficiency and poor reconstruction quality. In the current research, an underwater SPI system based on CS is established to reconstruct our two-dimensional (2D) transparent object. We have systematically investigated the influence of water turbid degree, measurement pattern types and number of measurements on image reconstruction performance. The proposed system is capable to reconstruct the object even when the turbidity reaches up to 80 Nephelometric Turbidity Unit (NTU), where the conventional imaging systems are unusable. Proposed reconstruction method in our research can save more than 70% data acquisition time, compared to SPI algorithm. Our experimental setup has been compared to a conventional imaging system and an underwater ghost imaging system to show its efficiency in obtaining accurate results from turbid water conditions. Furthermore, various algorithm comparison and imaging enhancement studies demonstrates that our algorithm is superior in bringing highly convex optimization at a faster rate with a smaller number of measurements. This work creates new insight into the SPI application and generates a guideline for researchers to improve their applications.

INDEX TERMS Single pixel imaging, compressive sensing, gated techniques, imaging through turbid media.

I. INTRODUCTION

Imaging in an underwater environment is difficult particularly in turbid media due to backscattering and absorption effects. Various researches have been done aiming to capture the images of objects in underwater environments [1], [2] and underwater imaging enhancement [3], [4]. Due to the presence of faster, more dynamic computers and strong fundamental spatial light mapping mechanisms such as Spatial Light Modulator (SLM) and Digital Micromirror Device (DMD) developed in the last decade comprehensive investigations have been done in the field of imaging which employs only a single pixel detector noted as Single Pixel Imaging (SPI) [5]–[7]. Compared to the conventional method, SPI makes it possible for the imaging system to use a low-cost single-pixel photodetector rather than an expensive multi-pixel Complementary Metal Oxide Semiconductors (CMOS) or Charge-Coupled Devices (CCD). It is convenient and efficient to manufacture single-pixel detectors with a large active area, which makes SPI techniques more appropriate for imaging, especially in low illumination conditions (underwater and foggy medium, etc.) than traditional

The associate editor coordinating the review of this manuscript and approving it for publication was Huimin Lu.

imaging techniques. The limited response of detection medium to a certain bandwidth has been a flaw of conventional imaging systems. The same drawback of the conventional system has become the major advantage of SPI because it can make measurement relatively in a much wider range of the electromagnetic spectrum. Consequently, the objective of SPI is to build an apparatus that is efficient for many real-world applications because of its ability to be a perfectly hyperspectral imaging system. With these exceptional strengths, extensive research attempts such as 3D [8]–[10], terahertz [11], [12], microscopy [13], remote sensing [13], scattering imaging [14], shadow less [15] and multispectral imaging [16] have been done to make use of its superiority. In addition, unlike conventional imaging system, SPI, a unique imaging technique by means of coincidence measurement using discrete intensity data has the feature of turbulence-free [17]–[19], low effect of backscattering [20]–[23] and wider angle of view (AOV) [24], [25], which can efficiently improve the underwater imaging performance.

SPI modulates both detection and illumination spatial signals into a one-dimensional (1D) light signal which make it possible to obtain spatial information only employing a single-pixel detector. The resulting 1D signals can be collected by a detector without spatial resolution, such as bucket detector or single-pixel detector. However, this scheme generally demonstrates a moderate frame rate, since to completely sample a target under investigation minimum required the corresponding measurement is at least the same as the number of pixels in the image reconstructed. To alleviate this, CS [26]–[28] has been introduced which take advantage of prior understanding to reconstruct the target from a pseudorandom measurement patterns deduced by the Digital Light Processing (DLP). It allows the reconstruction of the N-by-N pixel object using less than N^2 measurements.

However, there are limited studies which focus on applying SPI to capture the scene in the underwater environment and systematically analyzes the influence of turbidity on the system performance. Therefore, we attempt to exploit the advantages of SPI in an underwater environment for imaging in clear and turbid medium. Active SPI which is based on illumination modulation is chosen in order to analyze the performance in a water medium. This paper shows extensive investigation on SPI in an underwater environment of controlled turbidity by using a certain level of China clay and light transmittance meter. In order to fully capture the entire unknown scene to a specific resolution, the minimum number of measurements required is equal to the total number of pixels in the recovered image [29]. Therefore, the compression technique is used to reconstruct the image which is able to save sampling and calculating time and improve reconstruction quality efficiency. Our experimental results demonstrate that the proposed CS-based active mode underwater SPI is more reliable than the traditional underwater imaging techniques. It is able to recover the image when the medium turbidity reaches up to 80 NTU. In addition, more than 70% of the measurement time can be saved compared to the conventional method.

We first briefly introduce the underwater SPI and CS in the second section. In the third section, we demonstrate recovered images for measurement pattern types, various turbidities, and the number of measurements. In addition, the evaluation of performance, comparison study with conventional methods and results obtained using different methods are illustrated in this section. Finally, our conclusions and future plans are given in the fourth section.

II. THEORY

The proposed underwater object detection and image acquisition process are shown in figure 1. The signal strength of the object that has to be imaged is set as N which represents the total number of pixels in our reconstructed image. For the following step, the number of the observations (m) needed for reconstruction is calculated based on $m = O(K \log N)$. The sparsity of the binary matrix is important in the next step to limit the number of observations to m. The experiment will run until the number of measurements is equal to the number of observations. Then, l_1 minimization algorithm does the initial guess of the original signal X. This initial value is updated after each iteration of the l_1 minimization algorithm. The result is displayed in the final step.

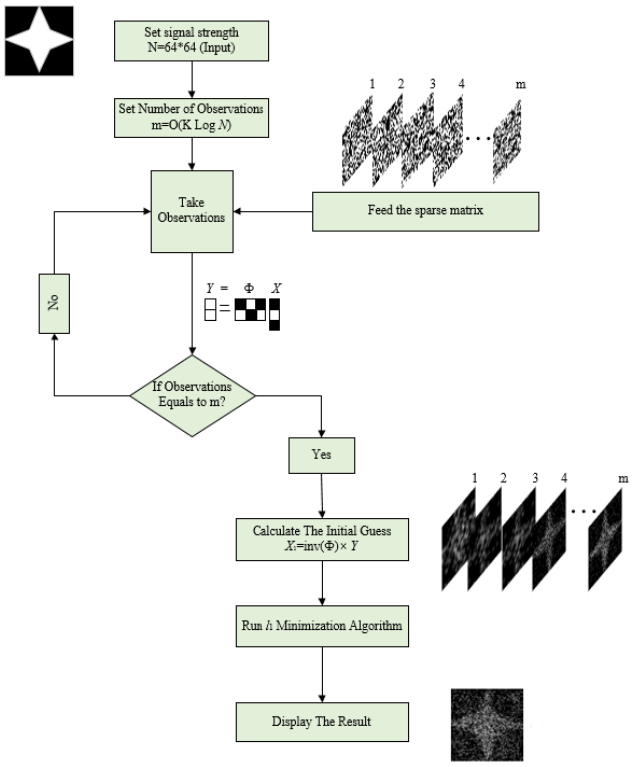

FIGURE 1. Summary of the proposed approach for underwater SPI.

SPI system works by gathering bucket sums of a light field which has interacted with an object under investigation and a spatial light modulator. The standard SPI system architecture

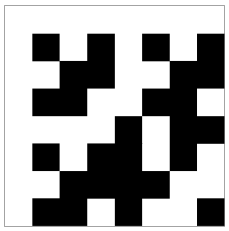

(a)

1	1	1	1	1	1	1	1
1	-1	1	-1	1	-1	1	-1
1	1	-1	-1	1	1	-1	-1
1	-1	-1	1	1	-1	-1	1
1	1	1	1	-1	1	-1	-1
1	-1	1	-1	-1	1	-1	1
1	1	-1	-1	-1	-1	1	1
1	-1	-1	1	-1	1	1	-1

(b)

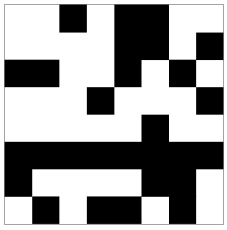

(c)

1	1	0	1	0	0	1	1
1	1	1	1	0	0	1	0
0	0	1	1	0	1	0	1
1	1	1	0	1	1	1	0
1	1	1	1	1	0	1	1
0	0	0	0	0	0	0	0
0	1	1	1	1	0	0	1
1	0	1	0	0	1	0	1

(d)

FIGURE 2. 8×8 Hadamard and random matrixes and corresponding binary patterns. (a) Hadamard pattern; (b) Hadamard matrix; (c) Random pattern; (d) Random matrix.

consists of following key components: a light source, optics, single pixel detector and Spatial Light Modulator (SLM). A series of generated patterns are used to illuminate the object by using SLM. The intensity value of each pattern is collected by single-pixel photodetector correspondingly, which is only sensitive to the intensity but not the phase of electromagnetic radiation. Tao et. *al* proved that binary patterns such as random and Hadamard patterns can modulate the light filed intensity effectively. Hence, it can be considered a suitable mask (measurement patterns) to illuminate the object [30]. As shown in figure 2 (b), the Hadamard matrix is a square matrix which is comprised of $+1$ and -1 where each row is orthogonal to another row. Figure 2 (a) shows the corresponding binary pattern to the Hadamard matrix, where white pixels represent $+1$ and black pixels represent -1. The random matrix consists of 0 and $+1$ determined through standard probability distributions like Gaussian or Bernoulli distribution. In this paper, we use Hadamard matrix as a projection pattern that contains $+$ 1 and -1 entries which corresponds to white and black pixel respectively. The 8×8 random matrix and its corresponding random binary pattern are given in figure 2 (c) and figure 2 (d).

In reality, the order of instruments in which the light beam communicated with the spatial light modulator and the object presents a significant separation between two conventions of operation unique to SPI system, namely active and passive mode SPI. The active mode arrangement is as follows: DLP, object, and detector. The passive mode arrangement is as follows: object, DLP, and detector. Our underwater system follows the active mode SPI. The schematic of underwater imaging system is shown in figure 3, which is built to form an image of thin transparent object 'four-point star'.

According to the definition, the patterns generated by the modulator (DMD) illuminates the object and results in the circulation of the intensity function Y that contains the product of corresponding X and Φ value at each pixel location. M-dimensional Column Vector Y and projected

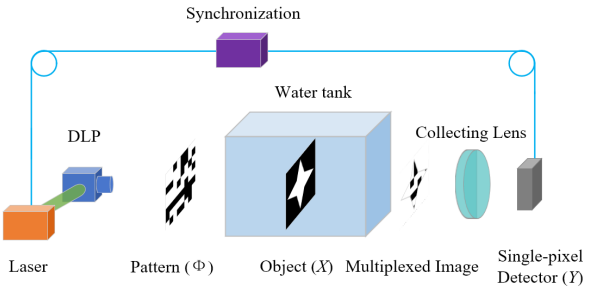

FIGURE 3. Sketch map of the experimental setup: underwater active mode SPI system. DLP: Digital Light Processing.

illuminating patterns can be concluded in terms of a single matrix equation:

$$Y_{M\times 1} = \Phi_{M\times N} \times X_{N\times 1} \tag{1}$$

in which, M represents the number of measurements, N is the dimension of the original signal and Φ is the measurement with dimension M×N. The unique solution of the Eq. (1) cannot be obtained by classical matrix inversion, which gives a unique solution for N×N matrices. However, when the measurement matrix Φ satisfies the Restricted Isometry Property (RIP) and sparse signal (X) is K−sparse, then the signal can be recovered by employing l_1 norm minimization problem with large probability and linear programming [31]. Practically, many signals do not exist with sparsity in their original form but can be represented sparsely in some suitable basis.

CS is a scheme for the simultaneous compression and sampling of sparse signals through incomplete, non-adaptive linear measurements [32]–[35], and the development of CS theory has brought tremendous progress in the research field of SPI. CS approach claims to retrieve certain signal and image using fewer measurements than conventional methods. Sparsity and incoherence are the two main keys behind the CS method. Sparsity and incoherence are related to interesting signal and sensing method, respectively. Sparsity represents a total number of non-zero elements in the signal transform domain. On the other hand, incoherence claims sensing and sampling waveforms possess an immensely dense presence in Ψ. The principle of incoherence states that the incoherent should be there between sensing and sparsifying basis. Considering the known basis, the sparsity of the measurement function and the precise solution of single pixel measurement, Eq. (1) can be achieved even if the measured number m is less than 30% of the object pixel number N [36]. According to this, there exists sparsifying basis Ψ ($\Psi = \{\psi_1, \psi_2 \ldots\ldots, \psi_N\}$) in N-dimensional space, the N-dimensional signal X ($X = \{X_1, X_2 \ldots\ldots, X_N\}$) is called to be K-sparse which can be expressed as:

$$X = \Psi S \tag{2}$$

where K belongs to non-zero entries in N×1 vector S and K is far less than N.

Regarding the CS theory, it is stated when the original signal image X contains such K-sparse basis, the signal can be recovered more than m ($m = \mathrm{O}(\mathrm{KlogN})$) incoherent linear measurements with high probability:

$$Y = \Phi X = \Phi \Psi S \tag{3}$$

in which, Φ is an M×N measurement matrix which is incoherent with the sparsifying matrix Φ and Y is the M×1 measurement vector [35].

The matrix Φ is defined as the measurement matrix [35]. If the maximum magnitude of the elements of $\Phi\Psi$ is small, the incoherent property would be fulfilled that satisfies the condition $\|X\|_0 < \frac{1}{2}\left(1 + \frac{1}{\mu(\Phi)}\right)$ for a given matrix $\Phi \in \mathbb{C}^{m\times N}$ with $m < N$ to obtain the unique solution for $\Phi X = Y$ [34]. When Φ is a random basis, for example, scrambled block Hadamard Ensemble, pseudo-random sequence and Bernoulli binary vectors this condition is achievable [37], [38]. Random matrix is highly incoherent with respect to any given basis. Basis Φ is used for the sensing purpose of the object and Ψ for the representation of the object. Orthogonality between Φ and Ψ is not mandatory but convenient to solve the problem simply. This coherence between the basis can be represented as follows:

$$\mu(\Phi, \Psi) = \sqrt{n} \max_{1\le k,j\le n} \left|\left\langle \Phi_k, \Psi_j \right\rangle\right| \tag{4}$$

Thus, the independency between the columns of the given matrix calculates the maximum correlation exists between any two elements of Φ and Ψ. If correlated members involve in both Φ and Ψ as a consequence coherence will be large otherwise it will be small. This largest and smallest value pursue linear algebra which is $\mu(\Phi, \Psi) \in \left[1, \sqrt{n}\right]$ and compressive sampling primarily interested in low coherent combinations. So, the performance of coherence is totally clear; the lesser the independence between rows and columns of the matrix, the lesser would be the correlated information in the samples, resulting in a reduction in samples for bringing a unique solution, hence our focus is low coherence structures.

Since K-sparse sparsifying basis Ψ occurs in several signal types, such as normal images are sparse in wavelet DCT, or Fourier domain, the property is taken advantage in the compression standards like JPEG and JPEG2000.

The recovery of X is done based on l_1 minimization. The fast approximation is possible when a signal containing a lesser number of significant coefficients and all the other coefficients are set to be zero. This is known as the sparsity of the signal. All the natural images, audio, and video signals are sparse in some basis. Consider a sparse matrix $\Phi \in \mathbb{C}^{m\times N}$ which obeys restricted isometric property and for a k - sparse vector X, define $Y = \Phi X$ where X has only k significant coefficient. Then the l_1 minimization model is given by:

$$\min\{\|X\|_1 : \|\Phi X - Y\|_2 \le \gamma\} \tag{5}$$

in which, γ is the generic norm, $\gamma \ge 0$. Let $Y = \Phi X^{\wedge}$ where $X^{\wedge}$ is sparse and most of its coefficients are zero or near to zero, $X^{\wedge}(k)$ be the best approximation of X and X^* be the optimal solution, then the result for the Eq. (1) is bounded sparsity of the measurement matrix and it is given by:

$$\left\|X^* - X^{\wedge}\right\|_2 \le Ck^{\frac{1}{2}} \left\|X^{\wedge} - X^{\wedge}(k)\right\|_1 \tag{6}$$

$$\left\|X^* - X^{\wedge}\right\|_1 \le C \left\|X^{\wedge} - X^{\wedge}(k)\right\|_1 \tag{7}$$

where sparsity k can be set to the order of $m/\log(n/m)$ depending the type of matrix are in use, and C is a generic constant. The model is again extended for high stability:

$$\left\|X^* - X^{\wedge}\right\|_2 \le C\left(\gamma + k^{\frac{1}{2}} \left\|X^{\wedge} - X^{\wedge}(k)\right\|_1\right) \tag{8}$$

in which, $X^{\wedge} = X^{\wedge}(k)$ and γ=0. Then the exact recovery $X^* = X^{\wedge}$ is achieved when the process combines with relevant measurement matrix (Φ).

The gradient of the sparse images is able to be utilized by applying Total Variation (TV) minimization of images. The discrete gradient for a digital image X can be determined at pixel location x_{ij} [39]:

$$\begin{aligned} G_{ij} &= \begin{pmatrix} G_{h;ij}(X) \\ G_{v;ij}(X) \end{pmatrix} \\ G_{h;ij}(X) &= x_{i+1,j} - x_{i,j} \\ G_{v;ij}(X) &= x_{i,j+1} - x_{i,j} \end{aligned} \tag{9}$$

The TV of image X can be expressed as the summation magnitudes of $G_{ij}(X)$ at each location in image signal X:

$$TV(X) = \sum_{ij} \sqrt{G_{h;ij}(X)^2 + G_{v;ij}(X)^2} \tag{10}$$

Quadratic constraints of TV minimization has been proposed to yield more suitable visual quality than the l_1 optimization when retrieving images using noisy observations [39]:

$$\min TV(X) \tag{11}$$

$$\textit{subject to } \|\Phi X - Y\|_2 \le \varepsilon \tag{12}$$

Candes *et al.* summarized seven distinct data reconstruction optimization problems. The CS inverse problem has been solved using CS measurements and proposed software package (l_1_MAGIC) [40].

In our theoretical analysis part, we show a brief theoretical introduction of underwater SPI and CS. Influence of pattern type, number of measurements and turbid degree on system performance are studied in the experimental part. Eq. (1) summarizes the principle behind the CS-based imaging system design philosophy. Using CS, the object can be reconstructed with a fewer number of measurements than the number of pixel in the image by the optimization method described in the following reference [41], [42].

III. EXPERIMENT AND ANALYSIS

A. EXPERIMENTAL SETUP

Based on our own previous investigation and following published literature on it, it has been observed and well investigated that the object reconstruction result would be

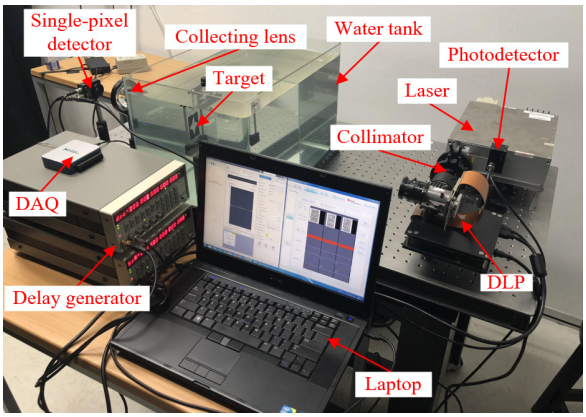

FIGURE 4. Experimental setups for CS-based underwater SPI.

greatly influenced by the noise of the light transmittance path. High power laser source has been implemented to increase the intensity of the light source. Laser, due to having high power with small divergence laser, the reflected light intensity value can be detected and captured easily by the single photodetector. In order to reduce the noise effect, we have synchronized the single pixel detector and the light source using gated technology and MATLAB software package. Using the discussed methods above, the light reflected from the object at a particular distance can be recorded by the DAQ (Data Acquisition). As shown in figure 4, emitted light from laser source illuminates the whole area of DMD, after beam shaping and spreading by using collimator. DLP (DLP Light Crafter 6500 Thorlabs) is used to illuminate the target by using random and Hadamard patterns generated by DMD chip mounted on it. The unit cell of random or Hadamard patterns shown onto the DMD is composed of 8×8 DMD pixels. A fraction of each pattern which passes through the object (a thin transparent 'four-pointed star') is collected by a collecting lens that concentrates light power at an effective area ($13mm^2$) of the photodetector (Thorlabs PDA36A-EC). Aiming to obtain intensity value, photodetector is connected to an analog to digital converter (A/D) (National Instrument USB-6001DAQ) to provides digitized signal from photodetector. Custom software developed in Matrix Laboratory (MATLAB) is capable of solving digitized CS measurements. Digital Light Projector is essential for projection of patterns and connected with the MATLAB. So, script .m MATLAB file has been created for connection through Internet Protocol/ Transmission Control Protocol (IP/TCP). The DAQ (Data Acquisition Toolbox) is useful to collect the data and MATLAB possesses functions to use National Instrument device (NI). A successful contact is required between the DLP and DAQ, a MATLAB code has been created for the automation and essentially for the synchronization of the data capturing procedure. The system ignores the possibility of attaching the wrong data to projected patterns. Contrary to time-based correspondence, DLP will only proceed next project matrix pattern after getting reading for the previous pattern. Synchronization process eliminations the probability of error and increases the measurements process systematically. Following minimization of the TV (min-TV), the image reconstruction is able to be completed in less than 15 seconds by MATLAB reconstruction algorithm [41].

In order to evaluate the reconstructed object images quality, we employ Peak Signal-to-Noise-Ratio (PSNR), and SSIM (Structural Similarity Index) which are regularly utilized to measure the reconstruction quality of images. Here, PSNR is defined as:

$$PSNR = 10 \cdot \log_{10}\left(\frac{MAX_I^2}{MSE}\right) \tag{13}$$

in which, MAX_I^2 is the maximum possible pixel value of the image when the pixels are represented using eight bits per sample, this value equals to 255. The MSE in Eq. (14) is the average squared difference between the original object and the reconstructed object image which can be given by:

$$MSE = \frac{1}{mn}\sum_{i=0}^{m-1}\sum_{j=0}^{n-1}[O(i,j) - R(i,j)]^2 \tag{14}$$

where, *O (i, j)* is the image of the object and *R (i, j)* is the reconstructed image. Additionally, m×n is the number of pixels in the comparison image.

SSIM is a unique approach to measure the analogy between the two captured photos. It is basically a matric which computes image characteristic deterioration induced due to operation such compression and data destruction in transmission. We have done all the related calculation on MATLAB. In which, we required two matrices reference and processed. The original image as a reference is the object image shown in figure 3. When calculating the PSNR and the SSIM index, we use MATLAB to generate a contrast image corresponding to the reconstructed image resolution while maintaining the reference image scale. and processed matric is compressed matrix. SSIM follows visible structures in the object compared to PSNR and SSIM is considered as a more reliable tool to measure the deterioration quality of images. The SSIM between $\mathbf{x}$ and $\mathbf{y}$ can be calculated with the following formulation:

$$SSIM(x,y) = \frac{(2\mu_x\mu_y + c_1)(2\sigma_{xy} + c_2)}{(\mu_x^2 + \mu_y^2 + c_1)(\sigma_x^2 + \sigma_y^2 + c_2)} \tag{15}$$

in which, μ_x and μ_y are the average of $\mathbf{x}$ and $\mathbf{y}$, σ_x^2 and σ_y^2 are the variance and σ_{xy} is covariance of $\mathbf{x}$ and $\mathbf{y}$. $c_1 = (k_1L)^2, c_2 = (k_2L)^2, k_1 = 0.01, k_2 = 0.03$. L is the range of pixel value [43].

B. RESULT AND ANALYSIS

1) EFFECT OF PATTERN

The reconstruction process can be affected by the nature and the type of distinct spatially with respect to the possible resolution, imaging speed, compressibility, and fidelity.

Hadamard and random patterns have been used in our observation for the reconstruction of the target image.

These patterns contribute large spatial frequency of the target. Binary patterns contain either 1 or 0 corresponds to full transmission and no-transmission, respectively. For grayscale patterns, it must vary between 0 and 1 for every pixel.

To observe the effect of pattern, images have been reconstructed using Hadamard and random patterns with different resolution (32×32, 64×64 and 128×128) with an equal number of measurements. Figure 5 (e) and figure 5 (f) show the reconstructed 128×128 resolution object in the same experimental condition (clear water) by projecting 500 random and Hadamard patterns of the same resolution. Recovered images using Hadamard patterns show better reconstruction in image quality the than the random ones, as edges are visible in figure 5 (f). From figure 5, reconstructed images employing Hadamard patterns are better for each resolution.

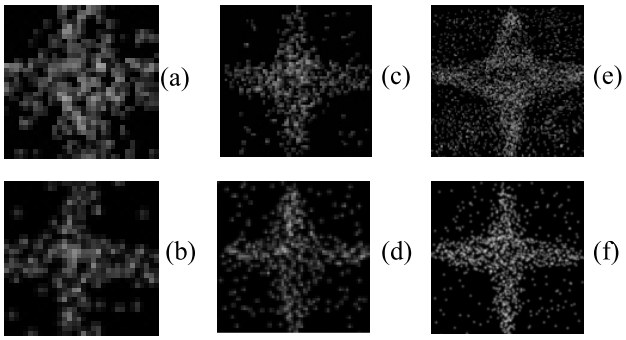

FIGURE 5. Recovered images with different resolution using random and Hadamard patterns in clear water under 500 measurements. (a) 32×32 random pattern; (b) 32×32 Hadamard pattern; (c) 64×64 random pattern; (d) 64×64 Hadamard pattern; (e) 128×128 random pattern; (f) 128×128 Hadamard pattern.

Using Eq. (14) and Eq. (16), PSNR and SSIM values of each reconstructed images in figure 5 are calculated and plotted in figure 6 and figure 7. A significant upward trend of PSNR and SSIM from 32×32 to 128×128 can be observed and PSNR corresponds to Hadamard patterns have a better response than the random patterns.

2) INFLUENCE OF THE NUMBER OF MEASUREMENTS

To investigate the influence of the number of measurements, different resolution objects are reconstructed in clean water using the Hadamard mode with different measurements (300, 500 and 1000 measurements), as shown in figure 8. When sampling objects, a small portion is missing due to noise and insufficient sampling. When the number of measurements is less than 20% of the total number of pixels using CS, the object can be reconstructed.

Figure 8 (g), figure 8 (h) and figure 8 (i) summarize that the reconstruction image becomes more reliable with the number of measurements increasing from 300 to 1000. From figure 8, it can be seen that figure 8 (c), figure 8 (f) and figure 8 (i) are the most reliable reconstruction with different resolutions.

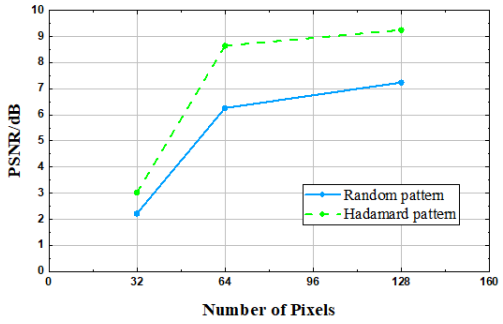

FIGURE 6. The plot of PSNR with different resolution under 500 measurements in clear water with respect to different projected pattern types.

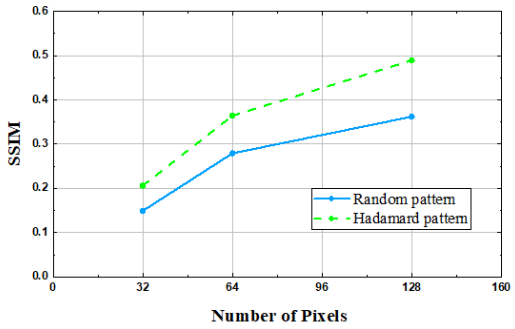

FIGURE 7. The plot of SSIM with different resolution under 500 measurements in clear water with respect to different projected pattern types.

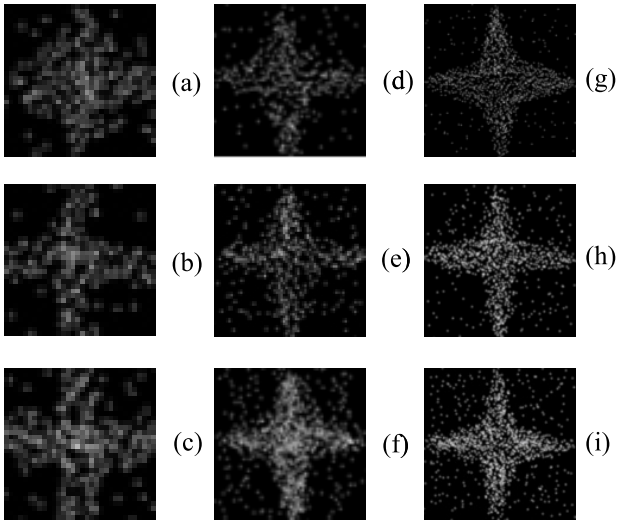

FIGURE 8. Recovered images with different resolution using Hadamard patterns in clear water under different number of measurements. (a) 32×32 300 measurements; (b) 32×32 500 measurements; (c) 32×32 1000 measurements; (d) 64×64 300 measurements; (e) 64×64 500 measurements; (f) 64×64 1000 measurements; (g) 128×128 300 measurements; (h) 128×128 500 measurements; (i) 128×128 1000 measurements.

Corresponding PSNR and SSIM of each recovered image in figure 8 are shown in figure 9 and figure 10 respectively. In these two figures, it can be observed that PSNR and SSIM

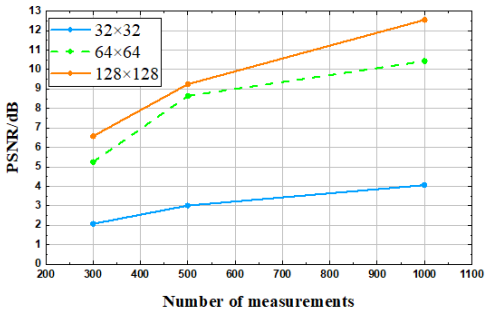

FIGURE 9. The plot of PSNR with different resolution under Hadamard patterns in clear water with respect to the number of measurements.

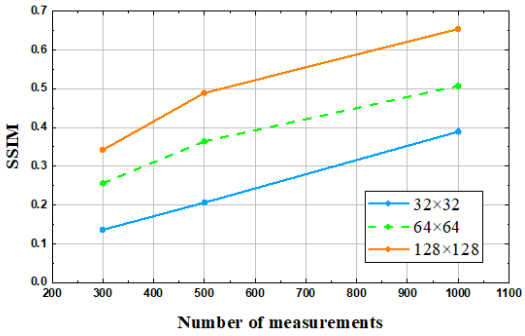

FIGURE 10. The plot of SSIM with different resolution under Hadamard patterns in clear water with respect to the number of measurements.

are proportional to the number of measurements which means reconstruction performance is higher for more measurements than with fewer measurements. Generally, it can be concluded that the more measurements we make, the more reconstructed images we get. Therefore, more sampling time should be performed to achieve better reconstruction performance in practical applications.

3) INFLUENCE OF TURBIDITY

The influence of turbid degree on the reconstruction quality will be discussed in this part. Instead of black ink, China clay is used to make the water have a different degree of turbidity. This increases the refractive index of the water, thus slowing the light travel.

According to previous studies, turbid water between the object and the light sensor has almost no effect on the quality of the image because the light sensor has no spatial structure and detects only the total light intensity. However, turbid water located between the light projector and the object distorts the light patterns and has a significant influence on the quality of the final image.

So, in our setup, turbidity is made uniform in the whole water tank irrespective of before and after the target to investigate the influence of turbidity. China clay is a chemical powder which can be mixed with the water and can generate absorption and backscattering to create turbidity. By controlling the amount of the China clay, the range of turbid degree of the water is from 0 NTU to 80 NTU, which is measured by using light transmittance meter. The increase in the refractive index of the turbid water is also measured using digital refractometer since it causes delay or shift in the detected light intensity. The DAQ device which is used to record the detected light intensity in the experiment is capable of recording the shift in detected light intensity.

Different reconstructed results within various turbid degrees (0, 20, 40, 80 NTU) under Hadamard illumination patterns of 1000 measurements are shown in figure 11. Comparing figure 11 (l) with figure 11 (i), figure (j), and figure 11 (k), a clear deterioration in reconstructed images can be observed with the turbid degree increasing from 0 NTU to 80 NTU. However, the reconstruction image remains distinctive even when the turbidity reaches as high

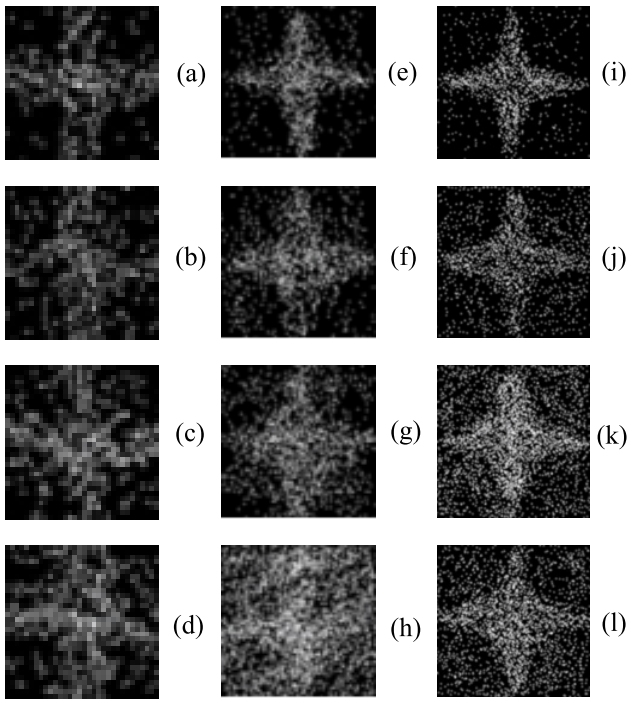

FIGURE 11. Recovered images with different resolution using Hadamard patterns in clear water under 1000 measurements. (a) 32×32 0 NTU; (b) 32×32 20 NTU; (c) 32×32 40 NTU; (d) 32×32 80 NTU; (e) 64×64 0 NTU; (f) 64×64 20 NTU; (g) 64×64 40 NTU; (h) 64×64 80 NTU; (i) 128×128 0 NTU; (j) 128×128 20 NTU; (k) 128×128 40 NTU; (l) 128×128 80 NTU.

as 80 NTU. PSNR and SSIM with respect to different turbid degrees for selected pattern resolution are summarized in figure 12 and figure 13. It can be evidently seen that the PSNR is proportional to the turbid degree which further proves the reconstruction performance decreases with increase in turbid degree. In addition, high-resolution pattern and more measurements can weaken the effect of the degree of turbidity. In extreme condition, for example, the water of high turbid degree, SPI can reconstruct the object provided enough number of measurements. It can be concluded that the SPI can be used as a novel solution of imaging over poor visibility environments such as turbid water, heavy fog and colloidal medium where conventional imaging method is thoroughly unavailable.

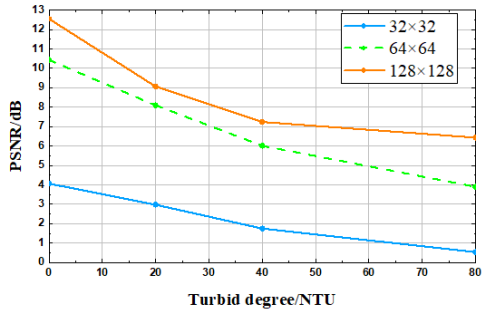

FIGURE 12. The plot of PSNR with different resolution under 1000 measurements and Hadamard patterns with respect to the turbid degree.

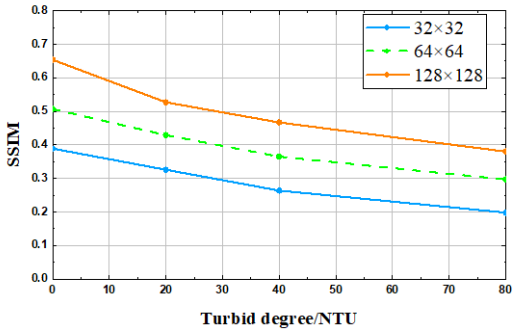

FIGURE 13. The plot of SSIM with different resolution under 1000 measurements and Hadamard patterns with respect to the turbid degree.

In all, our experimental results have shown better results with convincing reconstructed image quality with a smaller number of measurements. The results obtained is better than previously reported [42] results particularly in the turbid environment. Advantage of previously reported underwater ghost imaging is to cover a wide angle of view with the limitation in its insensitive response to change in turbidity.

4) COMPARATIVE EXPERIMENT WITH CONVENTIONAL IMAGING SYSTEM

The experiment setup of our gated conventional imaging system is illustrated in figure 14. A gated imaging system consists of a sensitive gated imaging camera and a pulsed illumination source.

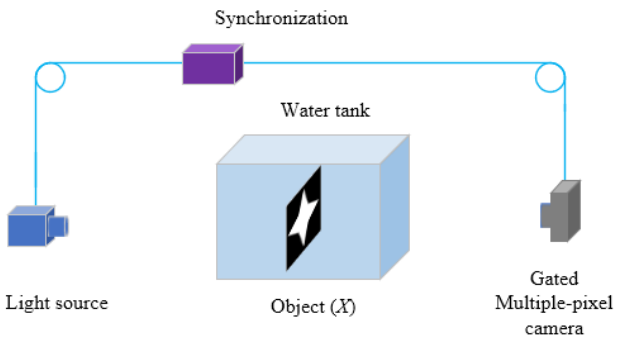

FIGURE 14. The schematic diagram of the experimental setup of the conventional imaging system.

In our system, a LED (Light-emitting Diode) pulsed light source is employed because most of the conventional imaging systems use a visible light source, and because of its fast switching specific characteristics we send a continuous square wave signal to the LED plane so that the effect of the stray light will be greatly reduced. In our experiment, the camera field of view (FOV) matches the light source divergence (DIV) and are matched to maximize the energy balance and, therefore, the range of the system. In our experiment white (6500K) high-power LED plane is chosen as the pulsed illumination light source which is pasted on the turntable and can be controlled by the synchronization system.

As illustrated in figure 14, the light pulse which travels through the depth of the scene will hit the object at a particular distance. Owing to the time of flight (TOF), the light photons hit the object first and then the camera in a fixed time. The camera aperture is closed when the photons travel towards it, and the camera delay generator will open the aperture after a certain delay and press the shutter for a short integration time. Therefore, the sensor of the gated camera will not be dazzled by backscattered photons or parasitic light sources. The sensor gate opens after a certain delay and for a short integration time. Thus, the light that arrived at the sensor within the right timing window is contributed to the imaging process.

Different captured images under different level of turbidity (0, 20, 40, 80 NTU) and refractive index are shown in figure 15. It can be seen that the conventional imaging system is highly affected by the turbidity and totally failed when the medium level of turbidity up to 40 NTU even in the case of using gated technology at the same time. So, it can be concluded that comparing to the traditional imaging system, SPI, a computational imaging system, can be used as a novel solution of imaging over poor visibility environments such as turbid water, heavy fog and colloidal medium where conventional imaging method is thoroughly unavailable.

5) COMPARISON INVESTIGATION WITH OTHER METHODS

After the analysis of our results, to evaluate the performance of the proposed method compared with other algorithms in terms acquisition time, quality of the recovered image and the number of measurements required for reconstruction, a series of investigation using different methods are conducted [44]. Figure 16 illustrates the results of the reconstructed object employing different methods.

As SPI is a linear system, to derive X from the set of measurements, different algorithms such as non-iterative methods, linear iterative methods, and non-linear iterative methods have been utilized. Among them, matrix inversion which is a non-iterative approach in which calculations are performed without any iteration. In this method, Φ^T is multiplied both the sides Eq. (1) and then X is calculated which is equivalent to minimizing l_2 ball when $m \geq N$ [45]. However,

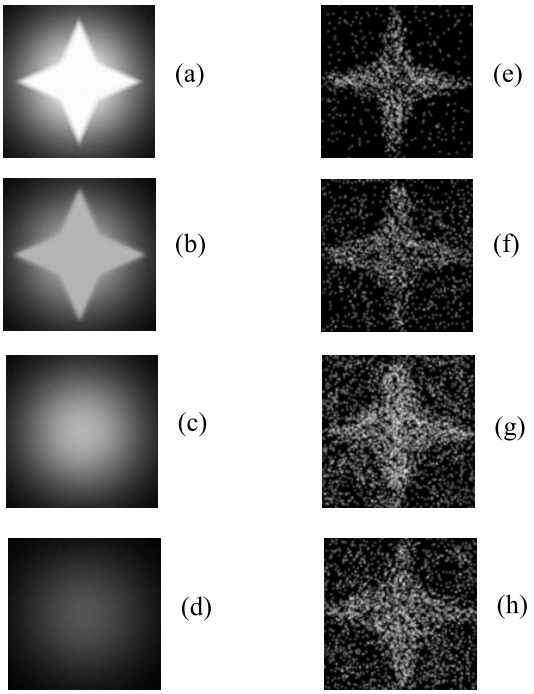

FIGURE 15. Comparison of the captured images using underwater SPI with a conventional imaging system. (a), (b), (c) and (d) are images captured by the conventional imaging system in different turbidity and (e), (f), (g) and (h) are reconstructed results using Hadamard patterns in different turbidity under 1000 measurements. (a) 128×128 0 NTU; (b) 128×128 20 NTU; (c) 128×128 40 NTU; (d) 128×128 80 NTU; (e) 128×128 0 NTU; (f) 128×128 20 NTU; (g) 128×128 40 NTU; (h) 128×128 80 NTU.

its application is limited in SPI since it won't work for $m < N$, i.e. $A^T A$ is non-full rank.

Gradient Descent, which is an iterative algorithm, finds a sparse solution for the SPI problem [46]. Restricted isometric property (RIP) of the measurement matrix should be satisfied to work with this approach. This algorithm solves for $X = H_s\left(X + \frac{1}{\gamma}\Phi^T r\right)$ where $\gamma = \delta_{2s} + \frac{1}{3}$ is RIP constant, Φ^T is the transpose of the measurement matrix, H_s is the operator which keeps the significant coefficient of Y and γ as residue. Though this algorithm ensures a unique solution to the problem, iterations through each and every X measurement increase the acquisition time.

We focus more on the robust and efficient non-linear iterative method which is l_1 minimization or least absolute deviations. It minimizes the sum of the absolute difference between Y and X. For the model $Y = \Phi X$, X is assumed to be k sparse and $X(k)$ is the approximation of X by setting $N - k$ coefficients of X to zero. In this method, the level of sparsity decides converging speed to a unique solution. Therefore, the right selection of measurement matrices which obey RIP and the incoherent property is needed. If we blow a l_1 ball, the probability of touching the tip of the ball (achieving a unique solution) is higher for high dimension real-time problems [47]. Our algorithm is compared with two other algorithms since the performance of the other algorithms which belongs to the class of non-iterative and linear iterative methods such as basis pursuit, orthogonal matching pursuit are consistent.

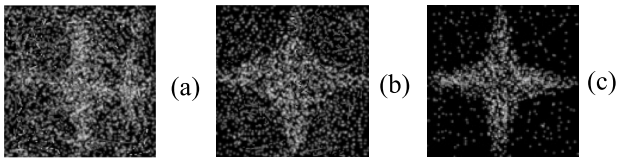

FIGURE 16. Recovered images in clear water with the different method with same resolution under the same number of measurements. (a) Matrix inversion 128×128 1000 measurements, (b) Gradient Descent 128×128 1000 measurements, (c) proposed method 128×128 1000 measurements.

In our comparison investigation part, we choose 1000 measurement values to reconstruct the object using different recovered methods we discussed above. Figure 16 (a) represents the result of the matrix inversion algorithm. This algorithm assures good quality results only for linear determined system. The result of the gradient descent algorithm is shown in figure 16 (b). This algorithm finds the optimized value by taking steps from an initial guess until it reaches to best or optimized value. The size of the steps is decided by the value in the residue. Though this algorithm gives far better result than the matrix inversion method, the time required for acquisition is much higher than compressive sensing based l_1 minimization. Since it iterates through each measurement by taking big or baby steps. However, l_1 minimization can produce good quality images with a few measurements, which is illustrated in figure 16(c). Restricted isometric property and sparsity of the signal make the acquisition faster in l_1 minimization that is explained which consistent with the discussion above.

6) CROSS-CORRELATION AND FILTERED METHOD FOR IMAGE QUALITY ENHANCEMENT

Based on experimental results, SPI produces a better result for different turbidity conditions. But the quality of the image is affected when the turbidity is 80NTU. To improve this situation, SPI is combined with conventional gated imaging techniques. In this experimental setup, the object is illuminated by a laser light source and the light transmitted through the objects is collected by a single pixel detector which has no spatial resolution. The other beam which is never interacted with the object is imaged by a CCD camera. Then the intensities obtained from the single pixel detector is correlated with the intensities of each pixel in the multi-pixel detector to obtain the image. The intensity correspondence of the single pixel detector and the CCD camera is calculated using the equation:

$$G_{m,n}(X) = \frac{1}{N}\sum_{i=1}^{N}\left[Y_0^i\right]^m\left[\Phi^i(x)\right]^n \tag{16}$$

where N is the number of samples and $I^s(x)$ is the s^{th} pattern at the reference detector. I_o^s is s^{th} signal of the bucket detector

and it is the obtained by the equation:

$$Y_o^i = \int dy O(y) \Phi^i(y) \tag{17}$$

where $O(y)$ is the object transmission function and $\Phi^i(y)$ is the pattern on the object arm. For conventional imaging technique, the number of measurements is equal to the number of samples, $m = n = N$. We also assume that the average size of the light falls on the object is about same as the pixel size of the conventional camera. Hence, the i^{th} signal of the single pixel detector is given by:

$$Y_o^i = \sum_{y_{in}}^{T} I^i(y_{in}) \tag{18}$$

in which, $I^i(y_{in})$ is the intensity of the signal within the coverage area of the camera and T is the number of illuminated pixels. The mean value of the cross-correlation function of the object and the reference signal is given by:

$$\left\langle G_{m,n}(x_{in}) \right\rangle = \frac{(T+m+n-1)!n!}{(T+n-1)!} \mu^{m+n} \tag{19}$$

$$\left\langle G_{m,n}(x_{out}) \right\rangle = \frac{(T+m-1)!n!}{(T-1)!} \mu^{m+n} \tag{20}$$

where x_{in} and x_{out} are the pixels of the camera that correspond to the pixels from the single pixel detector. To calculate the Eq. (19) and Eq. (20) we have used relations

$$\left\langle \left[\Phi^i(x) \right]^n \right\rangle = n\mu^n \quad \text{and} \quad \left\langle \left[\sum_{y_{in}}^{T} I^s(y_{in}) \right]^m \right\rangle = \frac{(T+m-1)!}{(T-1)!} \mu^m.$$

The combined technique of conventional and SPI is used for obtaining high-resolution images with good quality at 80NTU. The number of measurements required for reconstruction has increased to almost Nyquist limit since objects or images to be sampled at a rate twice the high-frequency component in conventional imaging to reconstruct images close to original ones. However, the result obtained is more significant and all the fine details of the object are imaged and recovered by combining these two methods.

From the four images in figure 17, it can be clearly observed that the results obtained using proposed combination method is close to that in case figure 15 (f) and is much better than that in cases figure 16 (a) and figure 16 (b). In other words, the negative effect brought by the environment turbidity can be well suppressed that enhanced the visibility of the target greatly. Furthermore, according to the experimental results above, it can be indicated that when the turbidity of the environment is not very high, only the SPI system proposed by us and the reconstruction algorithm based on CS can restore the target image well. At this time, the system is simple and has relatively high computational efficiency. Meanwhile, by combining gated techniques and cross-correlation methods, the noise of the achieved image is greatly reduced, and the quality is higher even when the object is in an extreme environment.

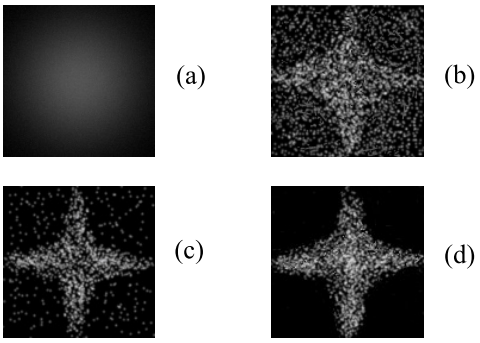

FIGURE 17. Captured object images with different systems. (a) Gated conventional imaging system; (b) Proposed active SPI system; (c) Cross-correlation method; (d) Filtered image.

The images obtained from the above method contain speckles and are non-uniform in intensity. It is removed without noticeably changing the original image to improve the quality when the water is more turbid. For the preprocessing of the images, median filtering can be applied to remove the speckle noise which arises in the detection and transmission process. The median filter is a non-linear filter which is widely used in image processing because of its edge keeping characteristics and its ability to reduce the speckle noise. The noise filtering characteristics depend on the size and shape of the filtering mask. The output of the median filtering is given by:

$$M(m,n) = med(G(m-i, n-j), \quad i,j \in W \tag{21}$$

where, i and j represent the rows and columns at a pixel location in $M(m,n)$ and $G(m,n)$ is the output image from cross-correlation method. W is the 2D mask which is of size 3×3. The noise-reducing effects of the median filter are depending on the size and shape of the filtering mask. Hence, the smallest possible size is taken for getting maximum quality. Figure 17 (d) is the filtered image, from where it can be clearly figured that the remaining background speckles are removed and edges are sharpened by the implementation of median filtering technique. In this filter, the neighboring value of the filtering mask will replace the noisy value of the image.

IV. CONCLUSION AND FUTURE WORK

In the current study, we proposed a system to demonstrate a novel underwater SPI application, which is beneficial for practical applications of underwater imaging. The proposed system employs random and Hadamard measurement patterns to reconstruct 2D transparent object image using CS. Following the CS approach, our system is capable to reconstruct the object with different resolutions (32×32, 64×64, and 128×128) using fewer measurements. Experimental results show that the reconstruction performance is proportional to the number of measurements. Therefore, a greater number of measurements are required to enhance reconstruction performance. This substantial reduction in the

number of measurements efficiently minimizes data acquisition time. A significant effect of Hadamard pattern compared with the random pattern on object reconstruction has been shown in this paper. Moreover, we show SPI can effectively weaken the effect of turbidity level, which could be considered for long-distance detection and imaging application. Our results are found to be better than conventional underwater imaging system, compared to the system described in figure 14. In the end, a comparative study is performed that clearly indicate our proposed system has better ability in approximating the original image quickly and qualitatively. Moreover, our systematic experiments and the imaging enhancement investigation illustrate that the proposed approach is suitable for underwater computational imaging, especially in extreme environments.

In the future to extend our research on underwater SPI, we will investigate the influence of other factors such as target characteristics, laser wavelength, required optics, and turbulence on imaging performance. We will also look into the solution to overcome the effect of turbidity we have discussed in this paper.

ACKNOWLEDGMENT

The authors gratefully acknowledge the support from School of Engineering, Monash University Malaysia.

REFERENCES

[1] A. Kanaev, A. T. Watnik, D. F. Gardner, C. Metzler, K. P. Judd, P. Lebow, K. M. Novak, and J. R. Lindle, "Imaging through extreme scattering in extended dynamic media," *Opt. Lett.*, vol. 43, no. 13, pp. 3088–3091, 2018.

[2] H. Lu, Y. Li, T. Uemura, H. Kim, and S. Serikawa, "Low illumination underwater light field images reconstruction using deep convolutional neural networks," *Future Gener. Comput. Syst.*, vol. 82, pp. 142–148, May 2018.

[3] Y. Li, H. Lu, K.-C. Li, H. Kim, and S. Serikawa, "Non-uniform de-scattering and de-blurring of underwater images," *Mobile Netw. Appl.*, vol. 23, pp. 352–362, Apr. 2018.

[4] H. Lu, Y. Li, L. Zhang, and S. Serikawa, "Contrast enhancement for images in turbid water," *J. Opt. Soc. Amer. A, Opt. Image Sci.*, vol. 32, no. 5, pp. 886–893, 2015.

[5] Z. Zhang, X. Wang, G. Zheng, and J. Zhong, "Fast Fourier single-pixel imaging via binary illumination," *Sci. Rep.*, vol. 7, no. 1, Sep. 2017, Art. no. 12029.

[6] S. Augustin, S. Frohmann, P. Jung, and H.-W. Hübers, "Mask responses for single-pixel terahertz imaging," *Sci. Rep.*, vol. 8, no. 1, Mar. 2018, Art. no. 4886.

[7] Q. Chen, S. K. Chamoli, P. Yin, X. Wang, and X. Xu, "Imaging of hidden object using passive mode single pixel imaging with compressive sensing," *Laser Phys. Lett.*, vol. 15, no. 12, Oct. 2018, Art. no. 126201.

[8] Z. Zhang and J. Zhong, "Three-dimensional single-pixel imaging with far fewer measurements than effective image pixels," *Opt. Lett.*, vol. 41, no. 11, pp. 2497–2500, 2016.

[9] M. J. Sun, M. P. Edgar, G. M. Gibson, B. Sun, N. Radwell, R. Lamb, and M. J. Padgett, "Single-pixel three-dimensional imaging with time-based depth resolution," *Nature Commun.*, vol. 7, Jul. 2016, Art. no. 12010.

[10] B. Sun, "3D computational imaging with single-pixel detectors," *Science*, vol. 340, no. 6134, pp. 844–847, May 2013.

[11] C. M. Watts, D. Shrekenhamer, J. Montoya, G. Lipworth, J. Hunt, T. Sleasman, S. Krishna, D. R. Smith, and W. J. Padilla, "Terahertz compressive imaging with metamaterial spatial light modulators," *Nature Photon.*, vol. 8, no. 8, pp. 605–609, Jun. 2014.

[12] W. L. Chan, K. Charan, D. Takhar, K. F. Kelly, R. G. Baraniuk, and D. M. Mittleman, "A single-pixel terahertz imaging system based on compressed sensing," *Appl. Phys. Lett.*, vol. 93, no. 12, Sep. 2008, Art. no. 121105.

[13] R. S. Aspden, N. R. Gemmell, P. A. Morris, D. S. Tasca, L. Mertens, M. G. Tanner, R. A. Kirkwood, A. Ruggeri, A. Tosi, R. W. Boyd, G. S. Buller, R. H. Hadfield, and M. J. Padgett, "Photon-sparse microscopy: Visible light imaging using infrared illumination," *Optica*, vol. 2, no. 12, pp. 1049–1052, 2015.

[14] E. Tajahuerce, V. Durán, P. Clemente, E. Irles, F. Soldevila, P. Andrés, and J. Lancis, "Image transmission through dynamic scattering media by single-pixel photodetection," *Opt. Express*, vol. 22, no. 14, pp. 16945–16955, 2014.

[15] S. Li, Z. Zhang, X. Ma, and J. Zhong, "Shadow-free single-pixel imaging," *Opt. Commun.*, vol. 403, pp. 257–261, Nov. 2017.

[16] L. Bian, J. Suo, G. Situ, Z. Li, J. Fan, F. Chen, and Q. Dai, "Multispectral imaging using a single bucket detector," *Sci. Rep.*, vol. 6, Apr. 2016, Art. no. 24752.

[17] N. D. Hardy and J. H. Shapiro, "Reflective ghost imaging through turbulence," *Phys. Rev. A, Gen. Phys.*, vol. 84, no. 6, Dec. 2011, Art. no. 063824.

[18] J. Cheng, "Ghost imaging through turbulent atmosphere," *Opt. Express*, vol. 17, no. 10, pp. 7916–7921, 2009.

[19] R. E. Meyers, K. S. Deacon, A. D. Tunick, and Y. Shih, "Virtual ghost imaging through turbulence and obscurants using Bessel beam illumination," *Appl. Phys. Lett.*, vol. 100, no. 6, Feb. 2012, Art. no. 061126.

[20] O. Bing, F. R. Dalgleish, F. M. Caimi, T. E. Giddings, J. Shirron, A. K. Vuorenkoski, W. Britton, B. Metzger, B. Ramos, and G. Nootz, "Compressive sensing underwater laser serial imaging system," *Proc. SPIE*, vol. 22, no. 2, Mar. 2013, Art. no. 021010.

[21] B. Ouyang, F. R. Dalgleish, F. M. Caimi, T. E. Giddings, J. J. Shirron, A. K. Vuorenkoski, G. Nootz, W. Britton, and B. Ramos, "Underwater laser serial imaging using compressive sensing and digital mirror device," *Proc. SPIE*, vol. 8037, Jun. 2011, Art. no. 803707.

[22] B. I. Erkmen, "Computational ghost imaging for remote sensing," *J. Opt. Soc. Amer. A, Opt. Image Sci.*, vol. 29, no. 5, pp. 782–789, 2012.

[23] Y.-K. Xu, W.-T. Liu, E.-F. Zhang, Q. Li, H.-Y. Dai, and P.-X. Chen, "Is ghost imaging intrinsically more powerful against scattering?" *Opt. Express*, vol. 23, no. 26, pp. 32993–33000, 2015.

[24] P. Zhang, W. Gong, S. Xia, and S. Han, "Correlated imaging through atmospheric turbulence," *Phys. Rev. A, Gen. Phys.*, vol. 82, no. 3, Sep. 2010, Art. no. 033817.

[25] A. K. Jha, G. A. Tyler, and R. W. Boyd, "Effects of atmospheric turbulence on the entanglement of spatial two-qubit states," *Phys. Rev. A, Gen. Phys.*, vol. 81, no. 5, May 2010, Art. no. 053832.

[26] E. Vera and P. Meza, "Snapshot compressive imaging using aberrations," *Opt. Express*, vol. 26, no. 2, pp. 1206–1218, 2018.

[27] F. Soldevila, V. Durán, P. Clemente, J. Lancis, and E. Tajahuerce, "Phase imaging by spatial wavefront sampling," *Optica*, vol. 5, no. 2, pp. 164–174, 2018.

[28] X. Ma, Z. Wang, Y. Li, G. R. Arce, L. Dong, and J. Garcia-Frias, "Fast optical proximity correction method based on nonlinear compressive sensing," *Opt. Express*, vol. 26, no. 11, pp. 14479–14498, 2018.

[29] D. B. Phillips, "Adaptive foveated single-pixel imaging with dynamic supersampling," *Sci. Adv.*, vol. 3, no. 4, Apr. 2017, Art. no. e1601782.

[30] T. Tao, *Structure and Randomness: Pages from Year One of a Mathematical Blog*. Providence, RI, USA: American Mathematical Society, 2008.

[31] S. Friedland, Q. Li, S. Dan, and E. A. Bernal, *Two Algorithms for Compressed Sensing of Sparse Tensors*. Cham, Switzerland: Springer, 2015, pp. 259–281.

[32] S. S. Chen, D. L. Donoho, and M. A. Saunders, "Atomic decomposition by basis pursuit," *SIAM Rev.*, vol. 43, no. 1, pp. 129–159, 2001.

[33] E. J. Candes and T. Tao, "Near-optimal signal recovery from random projections: Universal encoding strategies?" *IEEE Trans. Inf. Theory*, vol. 52, no. 12, pp. 5406–5425, Dec. 2006.

[34] E. Candès and J. Romberg, "Sparsity and incoherence in compressive sampling," *Inverse Problems*, vol. 23, no. 3, pp. 969–985, 2006.

[35] R. Baraniuk, "Compressive sensing," in *Proc. Inf. Sci. Syst.*, 2008, pp. 4–5.

[36] M. Rani, S. Dhok, and R. Deshmukh, "A systematic review of compressive sensing: Concepts, implementations and applications," *IEEE Access*, vol. 6, pp. 4875–4894, 2018.

[37] L. Gan, T. T. Do, and T. D. Tran, "Fast compressive imaging using scrambled block Hadamard ensemble," in *Proc. 16th Eur. Signal Process. Conf.*, Aug. 2015, pp. 1–5.

[38] T. T. Do, T. D. Tran, and L. Gan, "Fast compressive sampling with structurally random matrices," in *Proc. IEEE Int. Conf. Acoust., Speech Signal Process.*, Mar./Apr. 2008, pp. 3369–3372.

[39] E. J. Candés, J. K. Romberg, and T. Tao, "Stable signal recovery from incomplete and inaccurate measurements," *Commun. Pure Appl. Math.*, vol. 59, no. 8, pp. 1207–1223, 2006.
[40] D. Dudley, W. M. Duncan, and J. Slaughter, "Emerging digital micromirror device (DMD) applications," *Proc. SPIE*, vol. 4985, pp. 14–25, Jan. 2003.
[41] D. L. Donoho, "Compressed sensing," *IEEE Trans. Inf. Theory*, vol. 52, no. 4, pp. 1289–1306, Apr. 2006.
[42] E. J. Candes, J. Romberg, and T. Tao, "Robust uncertainty principles: Exact signal reconstruction from highly incomplete frequency information," *IEEE Trans. Inf. Theory*, vol. 52, no. 2, pp. 489–509, Feb. 2006.
[43] Z. Wang, A. C. Bovik, H. R. Sheikh, and E. P. Simoncelli, "Image quality assessment: From error visibility to structural similarity," *IEEE Trans. Image Process.*, vol. 13, no. 4, pp. 600–612, Apr. 2004.
[44] L. H. Bian, J. L. Suo, Q. H. Dai, and F. Chen, "Experimental comparison of single-pixel imaging algorithms," *J. Opt. Soc. Amer. A, Opt. Image Sci.*, vol. 35, no. 1, pp. 78–87, Jan. 2018.
[45] D. Shin, J. H. Shapiro, and V. K. Goyal, "Performance analysis of low-flux least-squares single-pixel imaging," *IEEE Signal Process. Lett.*, vol. 23, no. 12, pp. 1756–1760, Dec. 2016.
[46] D. G. Luenberger and Y. Ye, *Linear and Nonlinear Programming*, vol. 116. New York, NY, USA: Springer, 2008.
[47] Y. Zhang, "Theory of compressive sensing via ℓ_1-minimization: A non-RIP analysis and extensions," *J. Oper. Res. Soc. China*, vol. 1, no. 1, pp. 79–105, Mar. 2013.

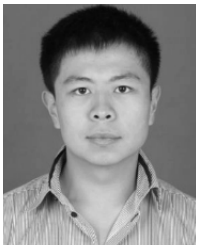

QI CHEN received the B.S. degree in geo-information science and technology from Hebei GEO University, China, in 2014, and the master's degree in instrument science and technology from the Changchun University of Science and Technology, China, in 2016, where he is currently pursuing the Ph.D. degree. He has been practicing as an Exchange Ph.D. Student at Monash University Malaysia, since January 2018. His research interests include laser-based underwater detection, single pixel imaging, and image processing.

SANDEEP KUMAR CHAMOLI received the M.Sc. degree in physics, in 2014, with specialization in electronics and laser physics. During M.Sc., he did his thesis work on experimental study of KTP optical parametric oscillator at DRDO, Dehradun. After getting good score in GATE–2015, he got opportunity to pursue M.Tech. degree from the Indian Institute of Technology Roorkee (IITR). During M.Tech., he prepared his thesis work on studies on liquid crystal-based optical waveguides and its sensing application. After submission of his M.Tech. thesis, he was an intern with DRDO on fabrication and simulation of lithium niobate-based rib waveguide, from June 2018 to August 2018. From October 2017 to June 2018, he was a Research Assistant with Monash University Malaysia Campus on single pixel imaging and laser sensing.

PENG YIN received the Ph.D. degree in engineering from the Changchun University of Science and Technology. He was a Visiting Scholar with Monash University Malaysia, from December 2018 to July 2019. His research interests include optical engineering and computing, laser sensing, and signal and image processing.

XIN WANG received the Ph.D. degree from Nanyang Technological University (NTU), in 2007. She was a Research Fellow with the Robotics Research Center, NTU, from 2007 to 2009. She was an Assistant Professor with the Faculty of Engineering and Science, Universiti Tunku Abdul Rahman, from 2009 to 2012. She is currently an Associate Professor with the School of Engineering, Monash University Malaysia. Her research interests include optical metrology, remote sensing, and machine vision.

XIPING XU received the B.S. degree in electronic engineering from the Changchun Optics Precision Mechanical School, China, in 1993, the M.S. degree, in 1999, and the Ph.D. degree from the Changchun University of Science and Technology, China, in 2004. He is currently a Professor and a Doctoral Supervisor with the College of Optoelectronic Engineering, Changchun University of Science and Technology. His research interests include image processing, signal processing, photoelectric detection technology, and modern photoelectric sensing technology.